Effects of boundary geometries on CFD simulations of recovery furnace char beds

Wenrui Yang, Robert R. Horton, and Terry N. Adams

ABSTRACT: Char bed behavior is an important aspect of recovery boiler operation. This paper presents results of several computational fluid dynamics (CFD) char bed models of different geometries, with emphasis on flow patterns and shear stress on the char bed surface. The effect of using steps in a Cartesian-coordinate grid to represent a smooth-sloped char bed surface is investigated. The geometries of the models examined include two-dimensional (2-D) models that are analogous to furnaces with slot air ports on two opposing walls, three-dimensional (3-D) slab models that are analogous to furnaces with air ports on two opposing walls, and a 3-D wedge model that resembles a furnace with air ports on all four walls.

Results of simulations with a Cartesian step surface and a body-fitted-coordinate smooth surface showed that both methods predicted similar flow patterns in the main gas phase, but the step-surface model underestimated shear stress and overestimated heat transfer area at the step boundary.

The 2-D and 3-D models predicted generally similar trends. However, significant differences have been found in results of different geometries.

KEYWORDS: Black liquor, fluid dynamics, fluid flow, fluid mechanics, furnaces, mechanics, recovery furnaces, simulation, spent liquors.

Char bed combustion in a black liquor recovery boiler is a complicated process involving fluid flow, chemical reactions, and heat and mass transfer. Interaction between a char bed and the air jets plays an important role in determining the shape of the bed and air flow pattern. Understanding char bed phenomena is important for stable furnace operation and furnace design improvements. Unfortunately, little information is available about gas-char bed interaction, since in an operating furnace, large dimensions, high temperature, and black liquor spray make most measurements very difficult. Physical modeling is restricted to cold flows and cannot simulate the effect of gas flow patterns on char bed formation and development *(1–4)*. Rapidly developing computational fluid dynamics (CFD) techniques provide a plausible means for research of this complicated char bed and flow interaction problem.

With advances in CFD software, CFD techniques have become a powerful tool for research on complicated fluid flow problems. CFD applications to recovery furnace simulations have produced valuable information about flow patterns and interactions of air jets *(4–12)*, trajectories of black liquor particles *(7, 13)*, interaction between black liquor spray and air flow *(14)*, and heat and mass transfer and chemical reactions *(6–8, 13, 15, 16)*. Simulation of char bed phenomena poses a greater challenge to CFD techniques. In addition to complicated transport and reaction processes, a char bed model involves a reacting boundary condition at the bed surface. The shape of the bed surface is determined by char arrival and consumption rates,

Yang is an assistant engineer, Horton is an assistant professor, and Adams is a professor at the Institute of Paper Science and Technology, 500 Tenth St., Atlanta, GA 30318.

which are not known beforehand. Recovery boiler CFD simulations have used assumed char bed shapes in the boundary conditions *(6, 16)*.

The large size of typical recovery furnace combustion zones relative to the small features of the furnaces, such as primary air ports, adds another difficulty to CFD modeling *(5, 7)*. An accurate CFD simulation of char bed phenomena requires large numbers of small computational cells to represent air ports and char bed shape accurately. This is very difficult for a model that includes the entire combustion zone, because the required total number of cells can easily become impractical for computer memory. Whole furnace models with less than 200,000 cells could only use one cell for a primary air port, or a slot for all the primary air ports *(5–7, 13)*. These models can predict gas flow patterns in the middle or upper combustion zones, but they are not accurate for char bed studies. Symmetry planes have often been used to simplify furnace models and reduce computational burden *(5, 8, 15)*. By using symmetry planes, simulations can focus on a small section of the char bed to increase resolution and numerical efficiency. When examining a small section of the overall flow problem, it is important to carefully impose boundary conditions, since they can influence simulation results.

1. Section of a typical recovery furnace char bed

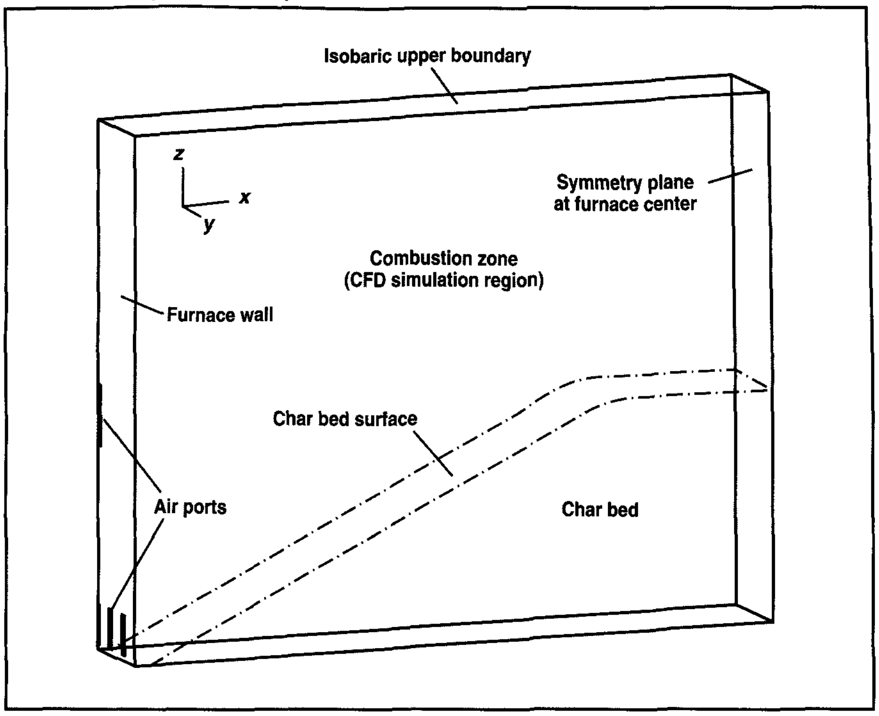

I. Summary of char bed models

Model	Grid type	No. of cells	Dimension	Geometry
2D-1	Cartesian	62x80	2-D	Large slot air ports
2D-2	BFC	62∞80	2-D	Large slot air ports
2D-3	BFC	67∞72	2-D	Air port area equivalent to 3-D models
SLAB-1	BFC	67∞72∞31	3-D	Uniform slice, rectangular air ports
SLAB-2	BFC	67∞72∞22	3-D	Uniform slice, slot primary air port
WEDGE	BFC	67∞72∞31	3-D	Wedge-shaped slice, rectangular air ports

In some CFD codes, computational grids can be set up in either Cartesian or body-fitted coordinates (BFCs). In Cartesian coordinates, a boundary that is not aligned with one of the grid lines must be represented by a series of steps. The error caused by the step boundary may seriously affect flow field calculations if the step size is comparable to the sizes of flow features *(4)*. Even with small steps, which have no serious influence on the gas flow patterns, the calculations of the surface transport processes may be in error. In comparison, BFC grid lines need not be orthogonal and can be aligned with boundaries, so the boundaries are smooth regardless of orientation *(17)*. Therefore, a BFC grid is more accurate than a Cartesian grid for irregular boundaries.

This paper presents a CFD study of jet flows near char beds in recovery furnaces. The effects of step and smooth char bed surfaces on gas velocity, shear stress, and heat transfer rates are examined. To understand the effects of specifying boundary conditions on simulation results, several simplified char bed models of different geometries are studied. The results provide useful information for selecting boundary geometries in more complicated simulations.

Description of char bed models

General description of a recovery boiler char bed

In this study, a typical, symmetric furnace geometry is considered. The horizontal cross section of the furnace is 10 m x 10 m. The primary air ports are 0.05 m wide and 0.3 m high, and are located on the walls at an elevation of 0.05 m, with intervals of 0.3 m. The secondary air ports are 0.15 m wide and 0.5 m high, and are located on the walls at an elevation of 1.5 m, with intervals of 1.5 m. Only the portion of the furnace below the liquor guns is considered. By using symmetry assumptions, the compu-

2. Cartesian-coordinate grid for Model 2D-1 with a step bed surface

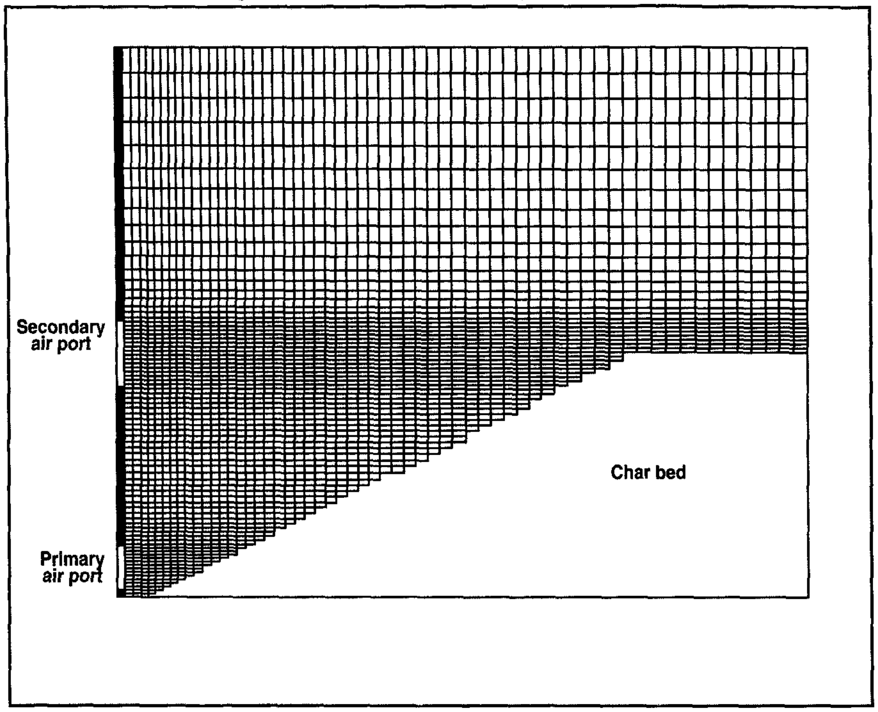

3. BFC grid for Model 2D-2 with a smooth bed surface

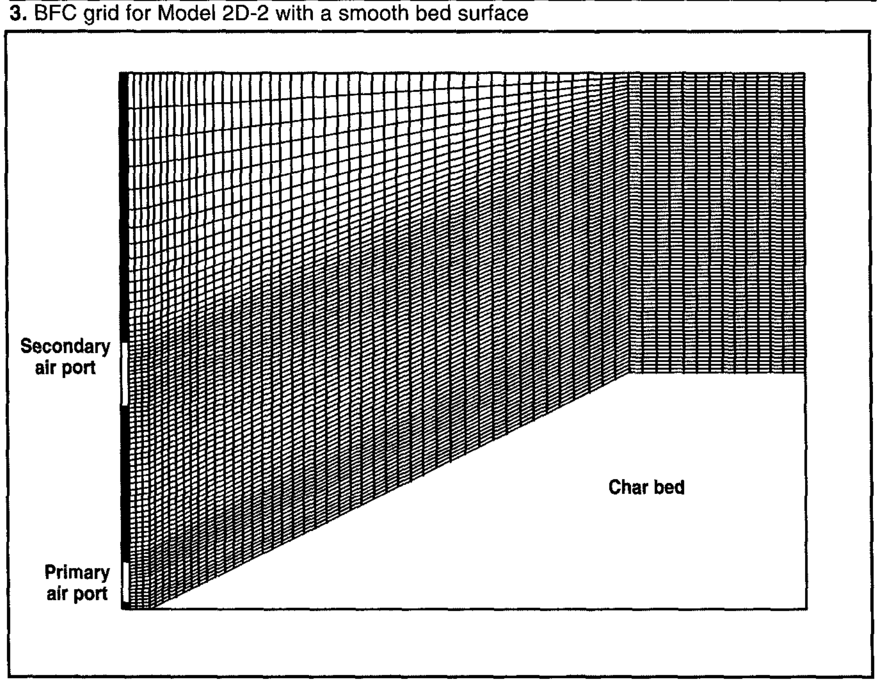

tational region is further reduced to a small section involving 2.5 primary and 0.5 secondary air ports, as is shown in **Fig.1**. The coordinate symbol indicates *x*, *y*, and *z* directions referred to in this paper. The char bed surface starts to rise at 0.15 m from the wall with a 1:2 slope and levels off at 3.7 m from the wall, resulting in a flat bed top that is 1.775 m high; the inlet air velocities are assumed to be uniform at the air ports. The primary air velocity is 50m/s in a 10° downward angle, and the secondary air velocity is 80 m/s in the horizontal direction. This results in an average vertical velocity of 1.3 m/s in any horizontal cross-sectional plane above the secondary air port in the region shown in Fig. 1. Heat transfer and chemical reactions are not considered in the present study, so an isothermal condition is assumed, and the physical properties of air at 1000°C are used.

Nonslip boundary conditions are used for the wall and the char bed. Fixed-velocity inlets are used for the air ports, and a fixed-pressure (isobaric) inlet is used for the upper boundary. The other boundaries of the slice are assumed to be symmetry planes. The standard κ-ε turbulent model is used.

The CFD code used in this work is FLUENT, version 4.11 *(18)*, which allows both Cartesian-coordinate grids and BFC grids *(17)*. The CFD code was run on an IBM RISC/6000 computer.

Geometries of char bed models

When simulating part of a furnace, imaginary planes that isolate the computational region from the rest of the furnace determine the shape of the char bed model. Six different geometries were examined in this study: three 2-D and three 3-D specifications. A summary of the models is given in **Table I.**

Two-dimensional Model No. 1 (2D-1). This 2-D model neglects variations in the *y* (thickness) direction, thus it corresponds to a furnace that has two infinitely long opposing walls with slot-type primary and secondary air ports. The slots maintain the original air port heights; therefore, the primaries are enlarged six times and the secondaries are enlarged ten times compared to the 3-D rectangular air ports. A Cartesian-coordinate grid with a step char bed surface, as shown in **Fig. 2,** is used in this model to study the effects of a step boundary condition.

Two-dimensional Model No. 2 (2D-2). This model has the same boundary specifications as Model 2D-1 except that a BFC grid with a smooth char bed surface is used, as shown in **Fig. 3**. Results from Models 2D-1 and 2D-2 are compared to show the similarities of and differences between the step and smooth boundaries.

Two-dimensional Model No. 3 (2D-3). Because of the enlarged air ports, results of the previous 2-D models are not comparable with realistic three-dimensional situations due to exaggerated flow rates. In Model 2D-3, the slot air ports are reduced in size so the air flow rates and the jet velocities are the same as those of the following 3-D models. Both the primary- and the secondary-slot air ports have a height of 0.05 m. Results from Models 2D-1 and 2D-2 show that gas velocity is very low in a region at the corner of the upper boundary and the wall. This allows the use of a partially sloped upper boundary to achieve more efficient node distributions in a BFC grid without noticeable influence on the gas flow patterns.

Three-dimensional slab Model No. 1 (SLAB-1). This 3-D model maintains the geometric features of the char bed illustrated in Fig. 1. Two parallel symmetry planes on both sides of the slab imply that the slab pattern repeats as mirror images in the *y* direction *ad infinitum.* This is equivalent to a furnace with air ports on two infinitely long opposing walls. A BFC grid is designed to provide higher resolutions for the air jets. A primary air port is represented by 36 (12 x 3) cells and the 0.5 secondary air port by 80 (16 x 5) cells.

Three-dimensional slab Model No. 2 (SLAB-2). This 3-D model has the same geometric features as the SLAB-1 model except that the primary air ports are replaced by a slot of the same total area. In the SLAB-1 model, a significant number of cells are needed to resolve the primary air ports. Since the primary air ports are closely spaced in a narrow band near the bottom of the wall, the primary air jets may mix in a short distance, and their contribution to the overall flow field may resemble that of a planar jet. By using a slot-type primary air port, the number of cells in the SLAB-2 model is reduced to 106,128 (67 x 72 x 22) from 149,544 in the SLAB-1 model. At the same elevation on the wall, the center of the slot air port is closer to the char bed surface than that of the rectangular air ports since the slot is shorter.

Three-dimensional wedge model (WEDGE). For a furnace with air ports on four walls, parallel symmetry planes between adjacent air jets do not exist due to interactions between air jets from adjacent walls. An accurate simulation of the air jet interactions must include a larger region with at least two adjacent walls. To include some effects of the air jets from the adjacent walls while maintaining the reduced size of the model, one of the symmetry planes in this WEDGE model is angled slightly so that the two side planes meet at the center of the furnace to form a wedge-shaped geometry, as shown in **Fig. 4**. As the air jets travel from the wall to the furnace center, the cross-sectional area reduces gradually to simulate air flow rate increase due to air jets from perpendicular walls. Strictly speaking, the WEDGE model corresponds to a nearly circular furnace with uniformly distributed air ports around the wall. Air jets in the middle of a symmetrical square furnace may correspond to a situation between the SLAB and the WEDGE models. The WEDGE model has the same inlet air flow rate as the SLAB models, but its average vertical velocity at the upper boundary is twice as large due to a smaller cross-sectional area.

4. Geometry of the WEDGE model

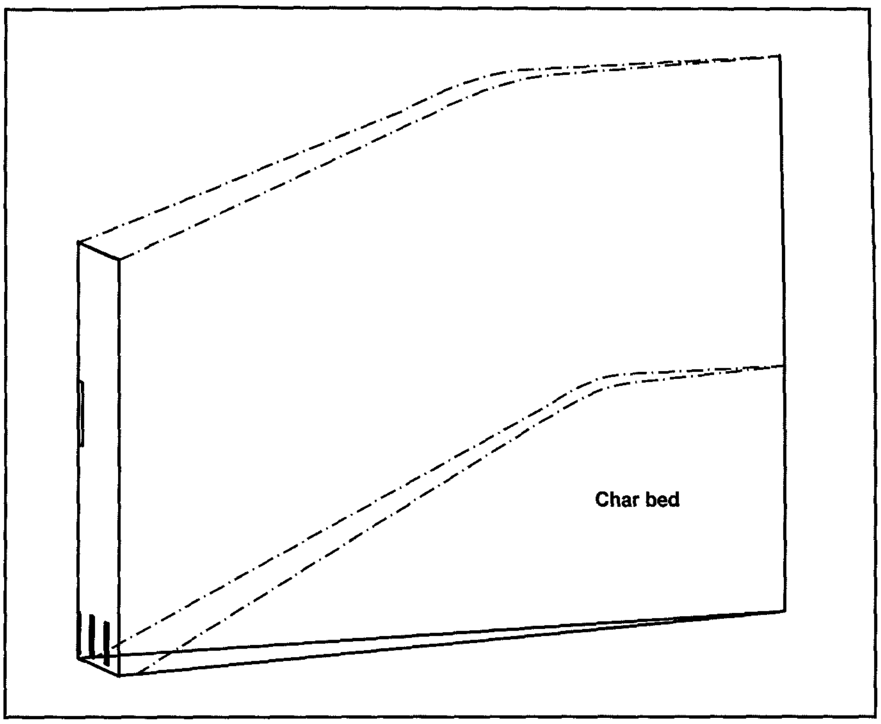

Grid sensitivity

Separate grid sensitivity studies have shown that node densities in this study were adequate for grid-independent solutions in nearly the entire computational region. However, turbulent kinetic energy and

5. Velocity magnitude for Model 2D-1 with a step bed surface. Gray scale = 0 – 80 m/s (dark – bright).

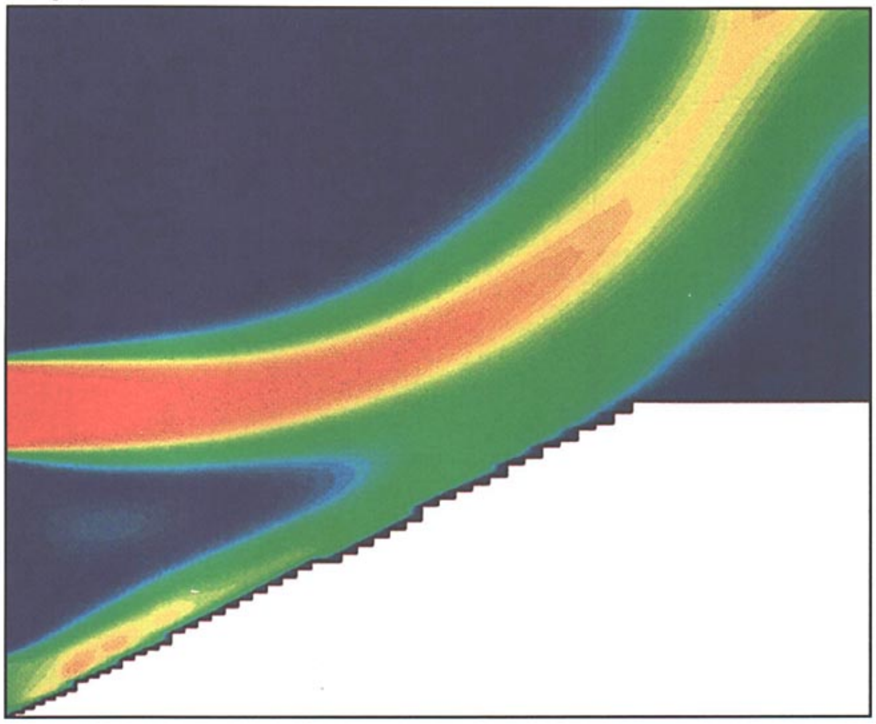

6. Velocity magnitude for Model 2D-2 with a smooth bed surface. Gray scale = 0 – 80 m/s (dark – bright).

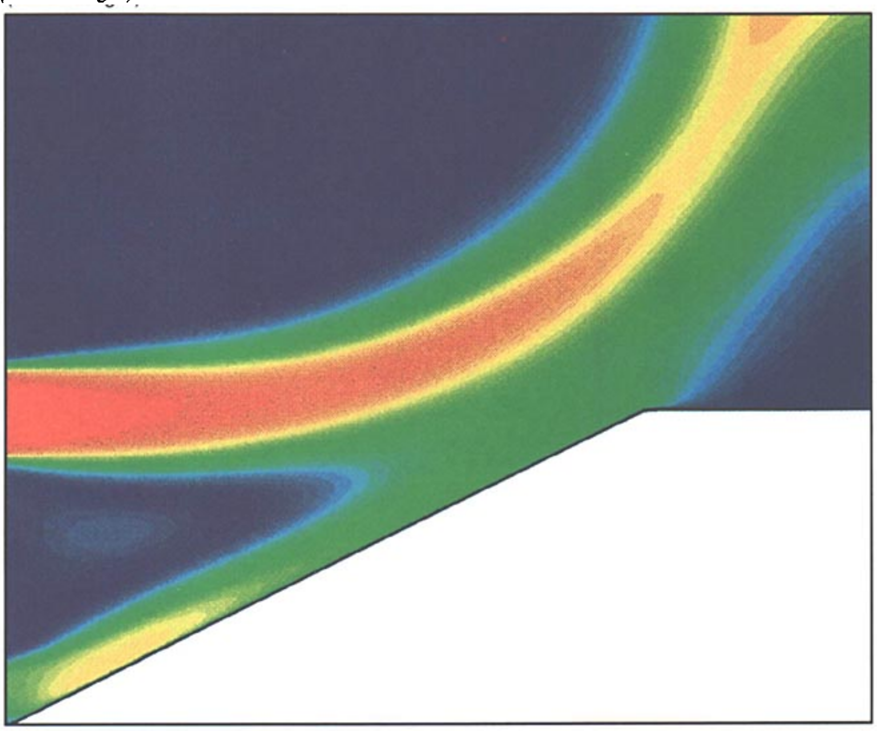

eddy dissipation rate were found to be grid-sensitive in very small regions at the edges of the air jet entrances. This was not due to inadequate node density in those regions, but rather due to the uniform inlet velocities that resulted in velocity discontinuity at the edges of the entering air jets. More practical velocity profiles should be used in the inlet boundary conditions to overcome this problem. In the present study, however, the effect of the velocity discontinuity is not important.

Results and discussion

Comparison between step and smooth boundaries

The velocity distributions for the step bed (2D-1) and the smooth bed (2D-2) models are shown in **Figs. 5 and 6**. The gray scale ranges from 0 in the darkest area to 80 m/s in the brightest area, and the same gray scale is used for all other velocity distribution patterns in this paper. Major flow features in both models, such as air jets and recirculation zones, are similar; however, the gas flow near the step surface is disturbed. The disturbance on the overall flow pattern is so small that it can be neglected for predicting velocities in the main gas phase.

The influence of the step boundary on calculating shear stress at the bed surface is significant. **Figure 7** shows distribution of the x component of the shear stress, τ_{wx}, on the step and smooth bed surfaces. For the smooth bed, the shear stress distribution profile varies smoothly, with a maximum at the area of primary air jet impingement. However, for the step bed, the shear stress distribution profile is markedly different, with smaller values and larger fluctuations. The average shear stress error on the step bed is 62% based on the shear stress of the smooth bed. Direct verification of the predicted shear stress is difficult due to the lack of experimental data. However, mass transfer rates on a smooth boundary calculated from predicted shear stress using the Chilton-Colburn analogy agree with experimental data reasonably well *(16)*.

The major shear stress difference between the step and smooth beds is caused by a velocity difference near the bed surface. In turbulent flow, a wall boundary layer consists of a very thin laminar sublayer and a "log-law" region, in which the flow is fully turbulent. In numerical calculations, the first node near the wall should be within the log-law region, and the wall shear stress is calculated via the log-law wall function *(18, 19)*:

$$u_p/u^* = (1/\kappa)\ \ln(Ey^+) \qquad (1)$$

where $u^* = \sqrt{(\tau_w/\rho)}$ is called the *friction velocity*, τ_w is the wall shear stress, u_p is the gas velocity at the first node (point p) near the surface, κ is von Karman's constant (0.42), E is an empirical constant (9.81 for a smooth wall), and y^+ is given by:

$$y^+ = (\rho\ k_p^{0.5}\ C_\mu^{0.25}\ y)/\mu \qquad (2)$$

where y is the distance from point p to the wall, k_p is the turbulent kinetic energy at point p, C_μ is an empirical constant (0.09), and μ and ρ are fluid viscosity and density, respectively. Equation 1 implies that u^* is proportional to u_p, i.e., τ_w is proportional to u_p^2 if y^+ is constant. This means that the shear stress is very sensitive to the gas velocity near the wall.

In the smooth bed model, the boundary grid lines exactly follow the char bed surface, and the calculations can be carried out for the cells adjacent to the surface. The resulting velocity distribution is smooth and consistent, as shown in **Fig.** 8. In the step bed model, the step surface deviates from the real surface. At cells adjacent to the surface, velocity tends to follow the step contour, which is misleading for the local gas flow, as shown in Fig. 8b. Cells located at the step corners are partially blocked by wall surfaces that do not exist in reality; consequently, the velocity near the surface is underestimated, resulting in erroneous shear stress predictions. Notice that, in Fig. 8b, one of the steps faces two horizontal cells, causing a large variation in predicted velocity. Such a variation causes a spike-like pattern in the shear stress distribution of Fig.7.

7. Comparison of shear stress distributions on step and smooth bed surfaces

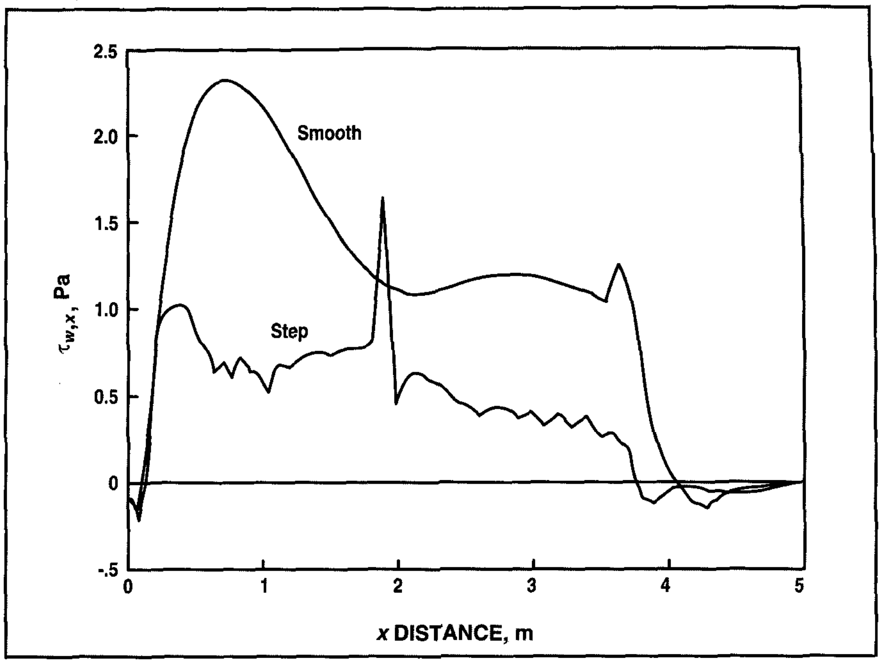

8. Velocity vectors near the step bed and the smooth bed

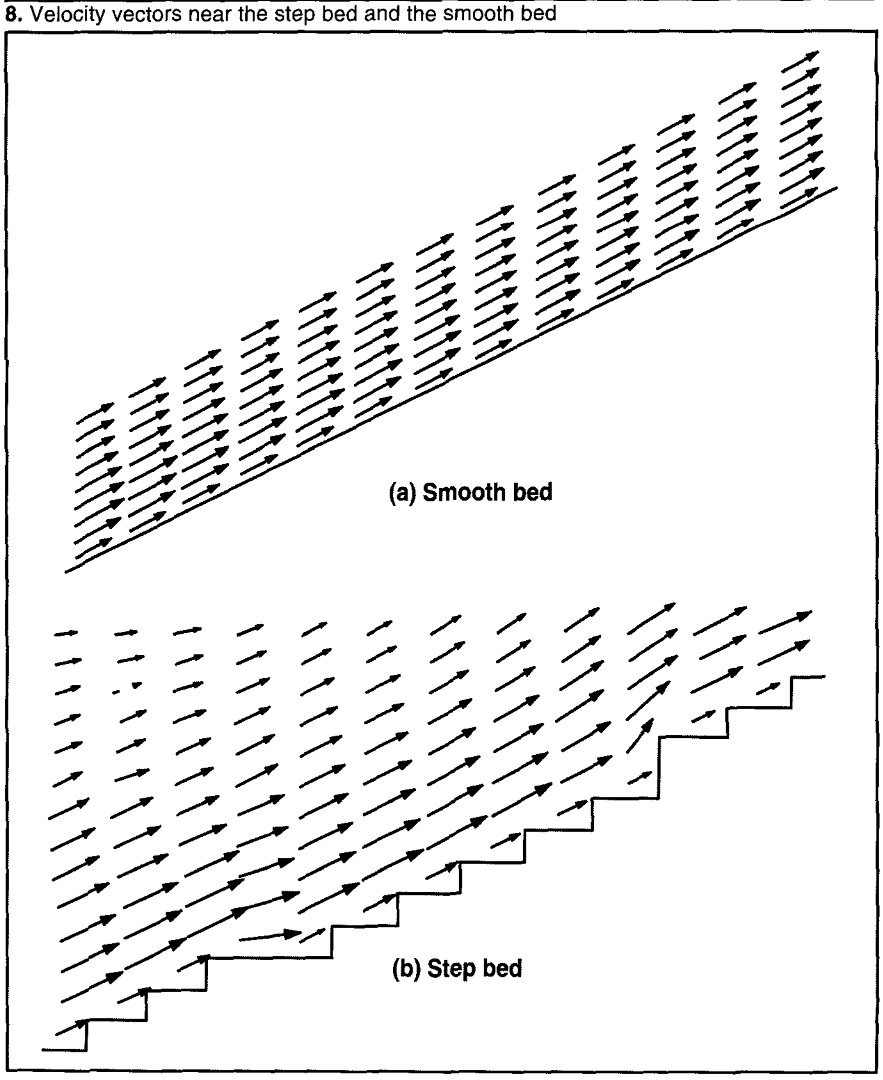

9. Heat transfer coefficients on step and smooth bed surfaces

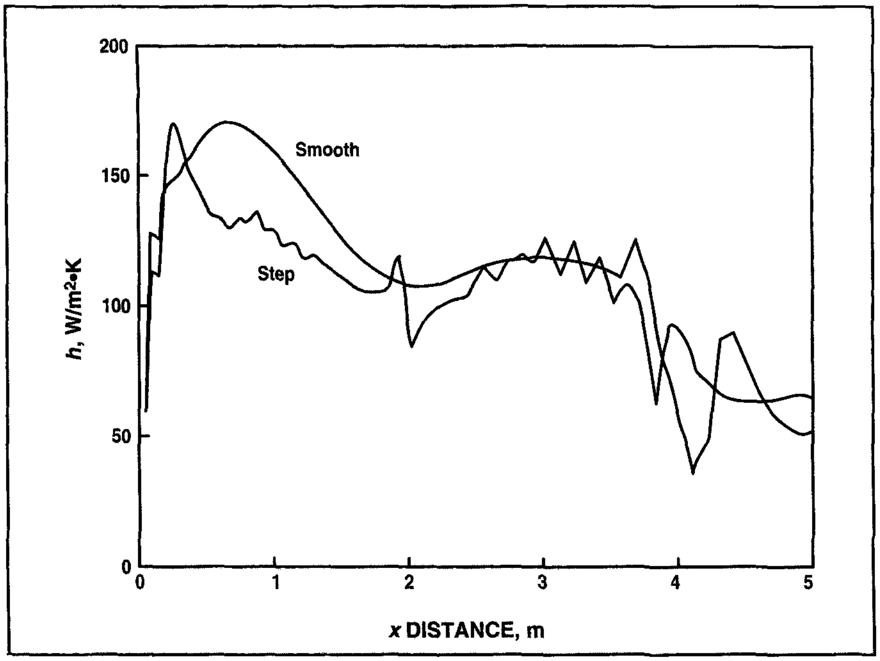

II. Heat transfer on the step and smooth beds

	Step bed	*Smooth bed*
Heat transfer area, m^2	6.8	5.4
Average heat flux, W/m^2	$4.7\infty10^4$	$4.9\infty10^4$
Overall heat rate, W	$3.2\infty10^5$	$2.6\infty10^5$

The influence of the step boundary on the shear stress remains as the step size decreases. As Eqs. 1 and 2 indicate, only the adjacent cells are used in calculating the shear stress. Regardless of how small the steps are, the cells at the step corners are always blocked by the step surfaces, causing the velocity to be inevitably underestimated.

An important application of shear stress calculation is predicting heat and mass transfer coefficients from the shear stress. For turbulent flows, the heat transfer to the wall is calculated by a log-law formulation that is based on the analogy between heat and momentum transfer *(18)*:

$$\frac{k_f/y}{h} = \frac{1}{\kappa y^+}\frac{\mathrm{Pr}_t}{\mathrm{Pr}}\ln(Ey^+) + \frac{\pi/4}{\sin(\pi/4)y^+}\left(\frac{A}{\kappa}\right)^{1/2}\left(\frac{\mathrm{Pr}_t}{\mathrm{Pr}}\right)^{5/4}\left(\frac{\mathrm{Pr}}{\mathrm{Pr}_t}-1\right) \quad (3)$$

where k_f is the thermal conductivity of the fluid, h is the heat transfer coefficient, Pr is the molecular Prandtl number, Pr_t is the turbulent Prandtl number (1.2 in the log-law region), and A is the vanDriest constant (26). Notice that velocity (u_p) is not included in the equation. The heat transfer coefficient depends on the turbulent kinetic energy and temperature, which determine y^+ and physical properties.

The previous isothermal models (2D-1 and 2D-2) were modified to include heat transfer calculations. In the heat transfer models, the wall and the char bed temperature is 800°C, and the inlet air is 100°C. The smooth bed model converged (sum of residuals < 10^{-3} and enthalpy residual < 10^{-6}) in 3900 iterations (6.7 hours CPU time), whereas the step bed model approached a stable solution with a large enthalpy residual (4×10^{-3}) after 50,000 iterations (60 hours CPU time).

Shear stress distribution patterns for the nonisothermal cases are very similar to those for the isothermal cases. **Figure 9** compares the heat transfer coefficients of the step and smooth surfaces. These coefficients are comparable except in the area impinged by the primary air jet. The average heat transfer coefficient error on the step surface is 14%, based on the smooth bed model, compared with 64% for the corresponding shear stresses in the nonisothermal cases. This is because the heat transfer coefficient is less sensitive to the velocity than the shear stress. The most influential variable on the heat transfer coefficient is turbulent kinetic energy, which is weakly affected by the step boundary condition. Consequently, the average heat fluxes for the step and the smooth boundaries are similar, as shown in **Table II.** This does not imply that the step bed model is suitable for heat transfer calculations. As Table II shows, the heat transfer area of the step bed is 26% larger than that of the smooth bed; thus, the overall heat transfer rate of the step bed is 23% larger than that of the smooth bed.

Effects of boundary geometry on gas flow predictions

Figure 10 shows velocity distribution patterns for models of different boundary geometries. In all the cases, the secondary air jets dominate the gas flow patterns. Air jets from opposing walls (by symmetry) interact in the furnace central region and form high-velocity upward central cores. The primary air jets have relatively small influence on the main gas flow patterns, since they dissipate quickly as they flow along the bed surfaces.

10. Velocity distributions for models of different geometries. Gray scale = 0 – 80 m/s (dark – bright).

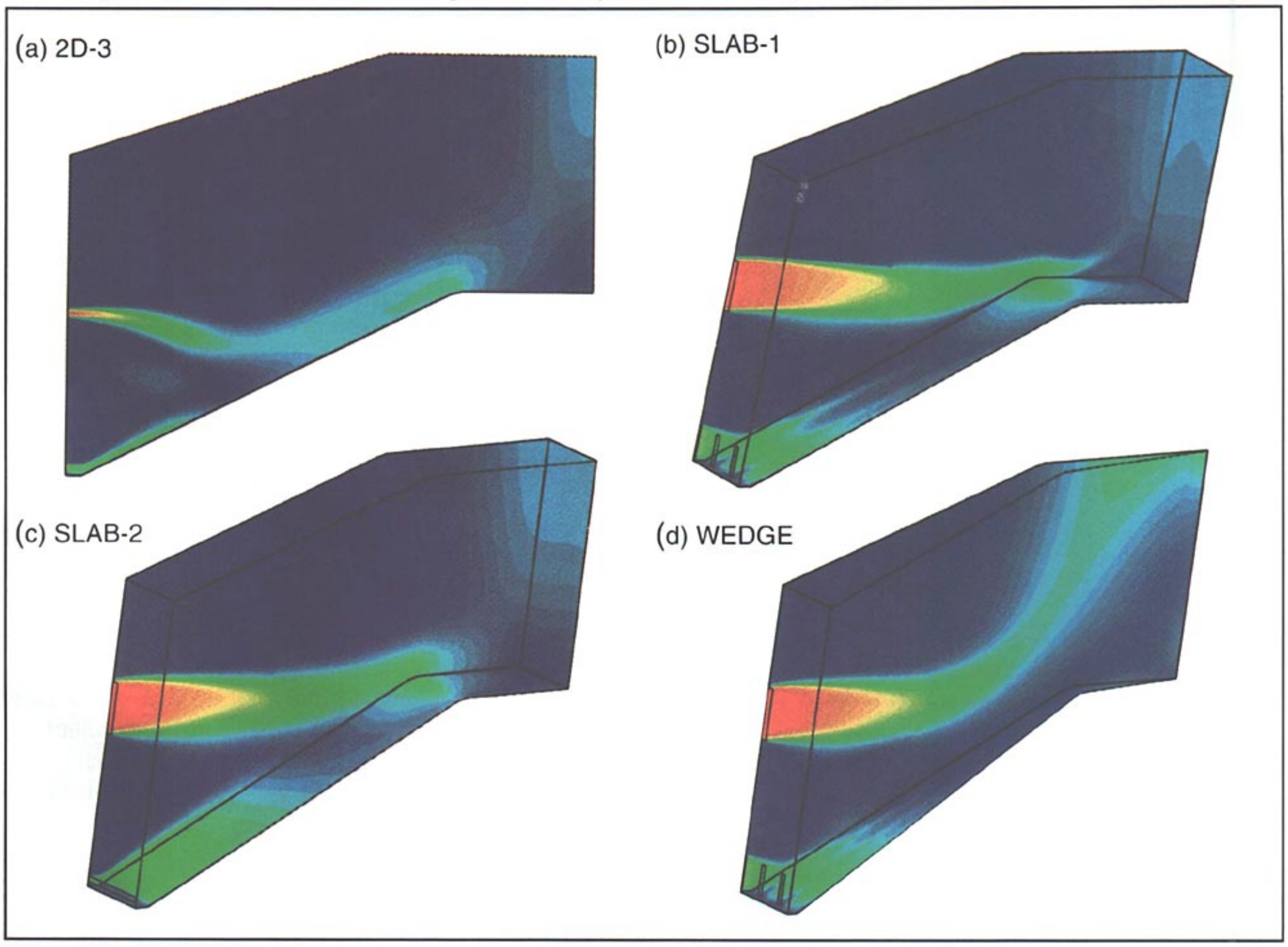

The boundary geometry has significant influence on the gas flow patterns. Generally, 2-D models are not suitable for predicting gas flow patterns in recovery furnaces because three-dimensional features are important for air jet flows. When simplifying 3-D rectangular air ports into a 2-D slot, we would either maintain the height of the air port and increase the air flow rate, as in Model 2D-1, or maintain the area of the air port and have a thinner planar air jet, as in Model 2D-3. Figures 6 and 10A show that neither of the 2-D models predicts a satisfactory flow pattern compared with the 3-D models in Figs. 10B–D.

Figures 10B and 10C show velocity distributions near the boundaries of the 3-D SLAB models. The secondary air jets extend horizontally

11. Comparison of average vertical velocities at the upper boundary

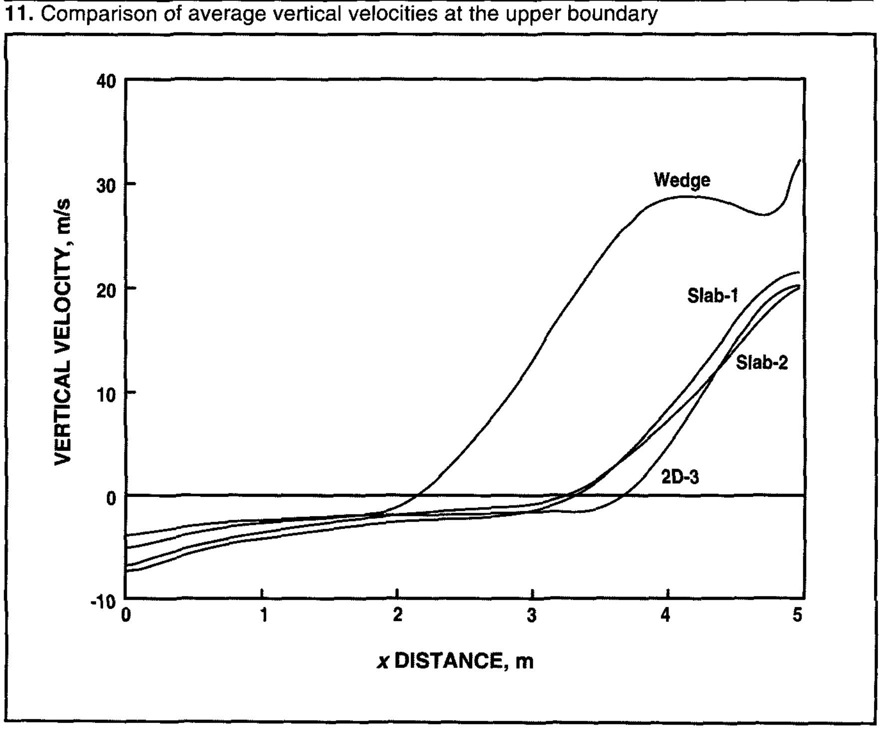

12. Patterns of shear stress distributions on char bed surfaces. Gray scale = 0 – 1.5 Pa (dark – bright).

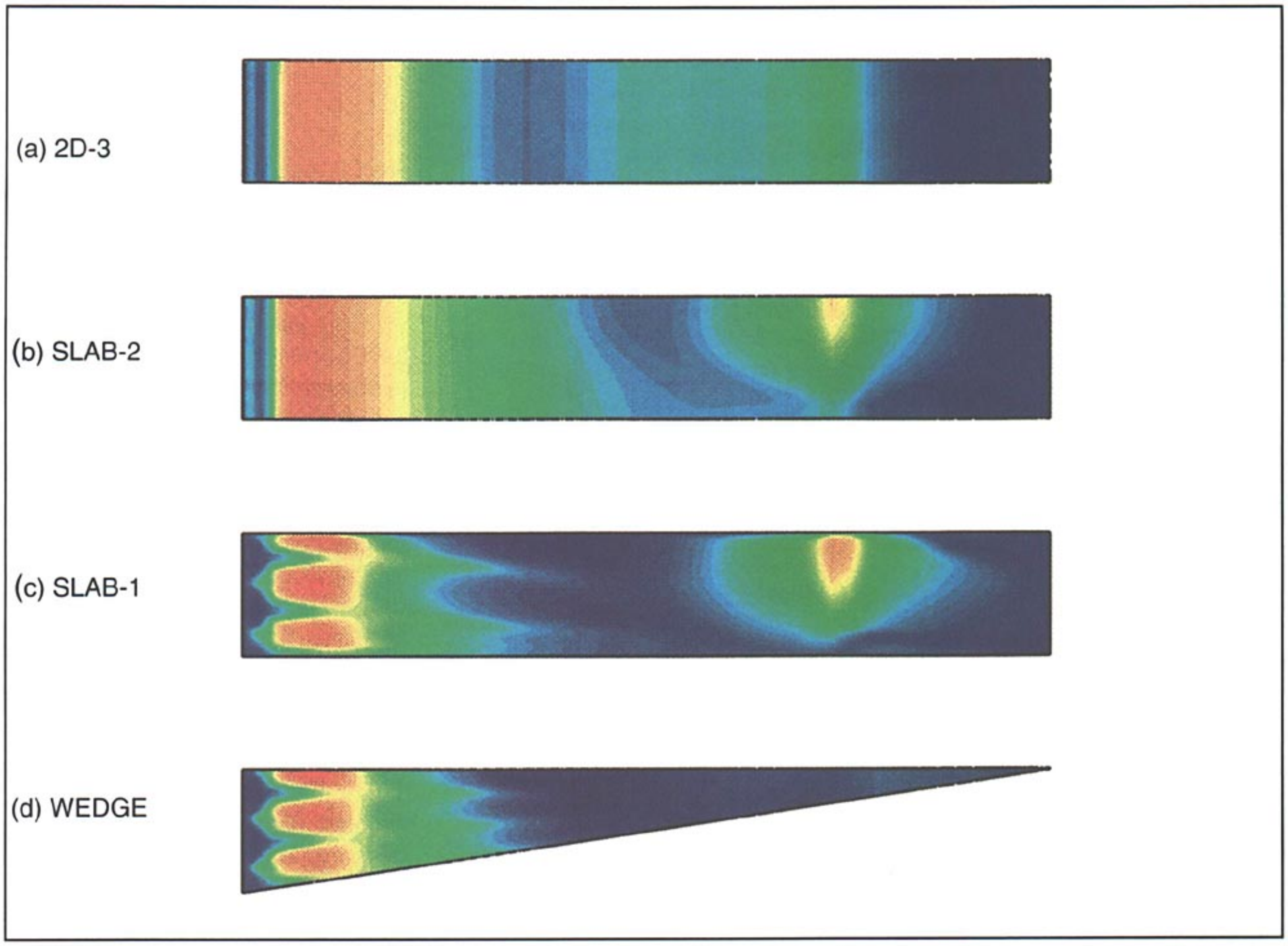

13. Comparison of average shear stress distributions on char bed surfaces

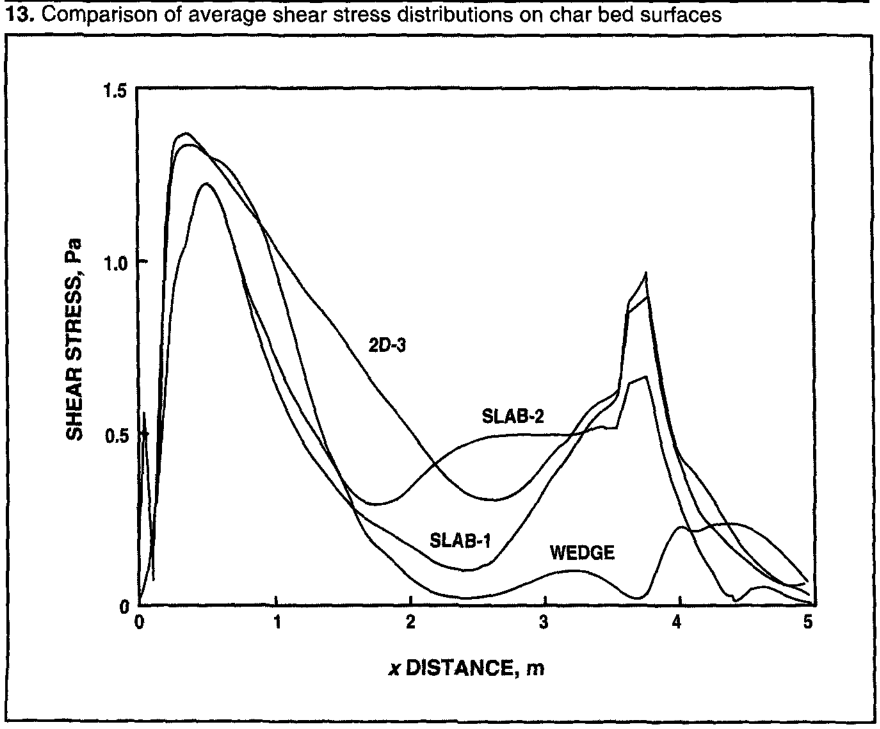

toward the center of the furnace. Model SLAB-1 has rectangular primary air ports. Upon impinging on the bed surface, the primary air jets are deflected, and adjacent air jets interact with each other, resulting in quick mixing. After a distance of about 1 m, the primary jets are well mixed as if the air came from a planar jet. By comparing Figs. 10B and 10C, we see that the primary air port geometry has little effect on the flow patterns except near the air ports. The planar jet dissipates slower and travels farther than the rectangular jets because it does not undergo the interaction process seen in the individual rectangular jets. This affects the calculations of the transport process on the bed surface.

The velocity distribution for the WEDGE model is shown in Fig. 10D.

The primary air jets dissipate in a short distance after impinging on the bed surface. Within this distance (one-third of the furnace depth), the wedge shape effect is small, and both the primary and part of the secondary air jets resemble those of the SLAB-1 model. At about half the distance to the center of the furnace, the converging side boundaries force the secondary air to turn upward before the main stream of the jet reaches the bed surface, resulting in a strong upward flow at the furnace central region. The WEDGE model includes the effect of flow rate increase due to air jets from the adjacent walls. It does not, however, include direct interaction of perpendicular air jets near the corners of a furnace. Therefore, this model is only suitable for a char bed section at the middle of a furnace wall, where the interaction between air jets is weak.

The models in the present study have symmetrical air port distributions, which inevitably result in higher velocities in the furnace's central region. The high-velocity central core may play an important part in particle entrainment and carryover *(13)*. **Figure 11** compares the average vertical velocities at the upper boundaries. The WEDGE model predicts higher velocities than the SLAB models because it has a smaller cross-sectional area, and the converging side symmetry planes force the air jet to turn upward sooner. It is not surprising that the SLAB models and Model 2D-3 predict similar velocity distributions at the upper boundary. The differences caused by the air port shapes gradually disappear as the air jets expand and mix. If the flow pattern of the primary air jets is not a major concern, using a slot-type primary air port configuration can save considerable computer memory and computational time.

Interaction of air jets with the char bed surface

Shear stress on the bed surface is an indication of the momentum transfer rate, which is analogous to heat and mass transfer *(19)*. Since the char bed combustion rate can be mass transfer limited *(20)*, the shear stress distribution has important implications for understanding the char bed phenomena. Higher shear stress indicates greater heat and mass transfer rates and, therefore, faster char combustion.

Figure 12 shows plan views of shear stress distributions on the bed surfaces. Model 2D-3 has been extended in the y direction to show the bed surface; the gray scale ranges from 0 Pa in the darkest areas to 1.5 Pa in the brightest areas. The maximum shear stresses are produced by the primary air jet impingements. Rectangular primary jets in the 3-D models produce high shear stress areas that are much wider than the air ports due to expansion of the air jets on the bed surface.

The effects of the secondary jets depend on the jet contact with the bed surface. In the WEDGE model, the main stream of the secondary jet does not touch the bed; therefore, its contribution to the shear stress is very small. In comparison, the secondary jets in the two SLAB models produce high shear stress areas at the top of the bed, where the air jets impinge on the bed surface.

The shear stress distributions, averaged in the y direction, are compared quantitatively in **Fig. 13**. The primary air jets produce comparable average shear stresses with the same air flow rate and initial velocity. The planar jets produce slightly higher average shear stresses than the rectangular jets, because the planar jet centers are closer to the bed surface. There is a large difference between secondary jet contributions of the WEDGE model and the SLAB models. In the WEDGE model, since the secondary jet turns away from the bed, the shear stress on the upper part of the bed is much smaller than that in the SLAB models.

Although the predicted velocity fields and shear stress distributions are related to the specific char bed geometries, there are still some common principles that are applicable to other char bed structures. The shear stress distributions suggest that the primary air jets are always important for the bed surface transport processes. The effects of the secondary air jets depend on whether they impinge on the bed surface. For a tall char bed that grows above the secondary ports, the secondary air may contribute significantly to the combustion at the top of the bed. If the bed is well below the secondary air ports, the secondaries may have no interaction with the bed.

Conclusions

This paper presents results of CFD simulations on recovery furnace char beds with different boundary conditions. The following conclusions can be drawn from the results.

Comparing a step bed model with a smooth bed model shows that a step boundary can be used to predict main gas phase flow patterns, but the velocity errors caused by the step boundary result in large errors in shear stress and heat transfer coefficient distributions. A step boundary overestimates the surface area and leads to an error in total heat transfer rate. A smooth boundary is recommended if the surface transport process needs to be accurately calculated.

Two-dimensional models are not suitable for predicting gas flow patterns quantitatively, because they cannot preserve important three-dimensional features of real furnaces. However, a planar primary air jet in a 3-D model may be acceptable for predicting flow patterns in the middle and upper combustion zones, since primary air port geometry has little effect on overall flow patterns away from the bed surface.

The SLAB models are suitable for furnaces with air jets on two opposing walls. However, the WEDGE model can include the effect of increased air flow rate due to perpendicular air jets and can be used for a char bed section in the middle of a furnace wall, where the interaction between the air jets is weak. More accurate simulations for interaction of perpendicular air jets must be carried out in larger regions involving at least two adjacent walls.

Primary air jets produce high shear stresses on bed surfaces; therefore, they are important in controlling bed shape. Air port geometries affect shear stress distributions. Therefore, they also affect mass and heat transfer processes, which play important roles in char bed combustion. TJ

Literature cited

1. Blackwell, B., *Tappi J.* 75(9): 122(1992).
2. Ketler, S. P., Savage, M. C., and Gartshore, I. S., *TAPPI 1992 Engineering Conference Proceedings,* TAPPI PRESS, Atlanta, p. 581.
3. Llinares, V. Jr. and Chapman, P. J., *TAPPI 1989 Engineering Conference Proceedings,* TAPPI PRESS, Atlanta, p.629.
4. Chapman, P. J. and Jones, A. K., *TAPPI 1990 Engineering Conference Proceedings,* TAPPI PRESS, Atlanta, p. 193.
5. Jones, A. K. and Grace, T. M., *TAPPI 1988 Engineering Conference Proceedings,* TAPPI PRESS, Atlanta, p. 3.
6. Sumnicht, D. W., "A Computer Model of a Kraft Char Bed," Ph.D. thesis, Institute of Paper Chemistry, Appleton, WI, 1989.
7. Chapman, P. J. and Jones, A. K., *1992 International Chemical Recovery Conference Proceedings,* TAPPI PRESS, Atlanta, p. 71.
8. Vakkilainen, E. K., Adams, T. N., and Horton, R. R., *1992 International Chemical Recovery Conference Proceedings,* TAPPI PRESS, Atlanta, p. 101.
9. Siiskonen, P., Karvinen, R., Hyoty, P., *et al., 1992 International Chemical Recovery Conference Proceedings,* TAPPI PRESS, Atlanta, p. 57.
10. Salcudean, M., Nowak, P., and Abdullah, Z., *1992 International Chemical Recovery Conference Proceedings,* TAPPI PRESS, Atlanta, p. 197.
11. Abdullah, Z., Nowak, P., Salcudean, M., *et al., TAPPI 1992 Engineering Conference Proceedings,* TAPPI PRESS, Atlanta, p. 103.
12. Quick, J. W., Gartshore, I. S., and Salcudean, M., *TAPPI 1992 Engineering Conference Proceedings,* TAPPI PRESS, Atlanta, p. 123.
13. Horton, R. R., Grace, T. M., and Adams, T. N., *1992 International Chemical Recovery Conference Proceedings,* TAPPI PRESS, Atlanta, p. 85.
14. Adams, T. N. and Horton, R. R., *TAPPI 1992 Engineering Conference Proceedings,* TAPPI PRESS, Atlanta, p. 81.
15. Karvinen, R., Hyoty, P., and Siiskonen, P., *Tappi J.* 74(12): 171(1991).
16. Sutinen, J. E. and Karvinen, R., *1992 International Chemical Recovery Conference Proceedings,* TAPPI PRESS, Atlanta, p. 79.
17. Anon., *PreBFC User's Guide, Ver. 4.0,* Fluent Inc., Lebanon, NH, December 1991, p. 151.
18. Anon., *FLUENT User's Guide, Ver. 4.0,* Fluent Inc., Lebanon, NH, December 1991, p. 190.
19. Incropera, F. P. and De Witt, D. P., *Fundamentals of Heat and Mass Transfer, 3rd edn.,* John Wiley & Sons, New York, 1990, p. 363.
20. Grace, T. M., Lien, S. J., and Brown, C. A., *1992 International Chemical Recovery Conference Proceedings,* TAPPI PRESS, Atlanta, p. 539.

This work was supported by the U.S. Department of Energy under contract No. DE-FG02-90CE40936 and IPST member company funding.

Received for review June 1, 1993.

Accepted Oct. 5, 1993.

Appendix

Nomenclature

- A = 26, van Driest constant
- C_μ = 0.09, empirical constant
- E = 9.81, empirical constant
- h = heat transfer coefficient, $W/m^2 \cdot K$
- k = turbulent kinetic energy, $(m/s)^2$
- k_f = thermal conductivity of fluid, $W/m \cdot K$
- Pr = Prandtl number
- Pr_t = turbulent Prandtl number
- u = velocity magnitude, m/s
- u^* = $\sqrt{(\tau_w/\rho)}$, friction velocity, m/s
- y = distance from the first node to the wall, m
- y^+ = variable in Eq. 2, dimensionless
- μ = viscosity, kg/m•s
- ρ = density, kg/m^3
- κ = 0.42, von Karman's constant
- τ_w = wall shear stress, Pa